Analysis and design recommendations for structures strengthened by prestressed bonded Fe-SMA

Lingzhen Li [a,b,*], Sizhe Wang [a,c], Eleni Chatzi [b], Masoud Motavalli [a], Elyas Ghafoori [a,d]

[a] *Empa, Swiss Federal Laboratories for Materials Science and Technology, Structural Engineering Research Laboratory, 8600 Dübendorf, Switzerland*
[b] *Institute of Structural Engineering (IBK), ETH Zürich, 8093 Zürich, Switzerland*
[c] *Singapore Center for 3D Printing, Nanyang Technological University, 639798 Singapore, Singapore*
[d] *Institute for Steel Construction, Faculty of Civil Engineering and Geodetic Science, Leibniz University Hannover, 30167 Hannover, Germany*

ARTICLE INFO

ABSTRACT

Previous studies have demonstrated a great potential of prestressed strengthening of structures employing iron-based shape memory alloys (Fe-SMAs). A bonded Fe-SMA strengthening solution with partial activation has been proposed. However, an analytical model for assessing the strengthening efficiency was lacking, due to the unique nature of the employed prestressing mechanism involving heating. In this study, a symmetric strengthening model and an asymmetric strengthening model are developed to analyze the prestress level in steel and glass beams and plates strengthened by bonded Fe-SMA strips. The asymmetric strengthening model is then modified to analyze reinforced concrete (RC) beams strengthened by embedded Fe-SMA rebars. Recovery stress at different activation temperatures, the influence of the activation temperature on the adhesive bond, as well as the prestress loss resulting from the deformation of substrate elements and adhesive joints are taken into account. The predicted strains and deflections in the parent structure closely approximate the experimental measurements that appear in current literature. A parametric study and a sensitivity analysis are then conducted to assess the impact of the four influential features on the final prestress level, and their impact is ranked in the following order: recovery stress ≈ Fe-SMA width > activation length > bonded anchorage length. Based on these findings, a design strategy, in line with Eurocode 0, for the bonded/embedded Fe-SMA strengthening system is proposed. Finally, some perspectives on potential areas for future research are offered.

1. Introduction

Metallic structures experience aging due to their exposure to cyclic loading (fatigue), increased service loads, and harsh environments [1]. The strengthening and retrofitting of existing metallic structures is intended to prolong their service life, reducing the demand for demolition and reconstruction, leading to a lower material and energy consumption [2,3]. Previous studies [4–7] have demonstrated the numerous benefits of prestressed strengthening of steel structures by employing iron-based shape memory alloys (Fe-SMAs), including ease of prestressing, satisfactory prestress level, the reasonable costs of the Fe-SMA material, and the possibility of re-prestressing. Most studies to-date focus on strengthening systems that employ mechanical anchors, such as mechanical fixtures [6,8] and nail fasteners [9].

In the cases where mechanical anchorages are not preferred, e.g. when no drilling holes to the parent structure are allowed, bonded anchorage systems offer a suitable alternative, which comes with the additional advantage of gradual stress transfer. Wang et al. [10] proposed a bonded Fe-SMA strengthening solution with partial activation, as illustrated in Figs. 1(a) and 1(b), where the middle segment of the Fe-SMA strip is heated to generate prestress, while the two ends remain unheated and transfer the prestress to the parent structure. Such a concept has been implemented in fatigue strengthening of central cracked steel plates [10,11], static and fatigue strengthening of steel beams [12,13], and flexural strengthening of glass beams [14,15].

Fig. 2 schematically shows the mechanism of prestressing Fe-SMA strips. (i) An Fe-SMA strip is tensioned to a prestrain level (ε_{pre}) and (ii) unloaded to a zero-stress state, characterized by residual strain (ε_{res}). These two steps are known as the prestraining process, after which the Fe-SMA strip is referred to as the prestrained Fe-SMA. The residual strain comprises a portion attributed to the austenite to martensite phase transformation strain (ε_{phase}) and a plastic strain

---

Nomenclature

X	Model input
Δ_a	Shear deformation of adhesive joint
Δ_s	Compressive deformation of steel plate/beam
$\Psi_\alpha(X)$	Multivariate polynomial basis
ρ	Stiffness ratio
σ_{loss}	Prestress loss
σ_{pre}	Prestress
σ_{rec}	Recovery stress
σ_{steel}	Compressive stress in steel plate
$\varepsilon_{bending}$	Bending strain component at edge of beam height
ε_{comp}	Compressive strain component at edge of beam height
ε_{phase}	Phase transformation strain
$\varepsilon_{plastic}$	Plastic strain
ε_{pre}	Prestrain level
ε_{res}	Residual strain
A_{SMA}	Cross-sectional area of Fe-SMA strip
A_{steel}	Cross-sectional area of steel plate
b_f	CFRP strip width
b_{SMA}	Fe-SMA strip width
E_f	CFRP E-modulus
E_{SMA}	Secant modulus of Fe-SMA strip in quasi-linear stage
E_{steel}	E-modulus of steel substrate
F_b	Bond capacity
$f_{F-\Delta}(\cdot)$	Nonlinear load–displacement curve of adhesively bonded joint
F_{SMA}	Tensile force retained by Fe-SMA strip
F_{steel}	Compressive force resisted by steel plate
G_f	Fracture energy of adhesive bond
h	Beam height
I	Beam moment of inertia
k_{joint}	Stiffness of the quasi-linear stage of $f_{F-\Delta}(\cdot)$
L_{act}	Half of activation length
L_{anchor}	Bonded anchorage length
L_{grad}	Distance between points of applied dipole forces and the closest pin support
M	Bending moment
R	Resistance
S	Action
S_T	Total Sobol index
t_f	CFRP strip thickness
T_{act}	Activation temperature
x	Coordinate in beam longitudinal direction
y	Deflection of beam
y'	Slope of beam
y''	Curvature of beam
$Y(X)$	Model output
y_α	Coefficients of polynomial expansion
CFRP	Carbon fibre reinforced polymer
FE model	Finite element model
Fe-SMA	Iron-based shape memory alloy
PCE	Polynomial chaos expansion
RC structure	Reinforced concrete structure
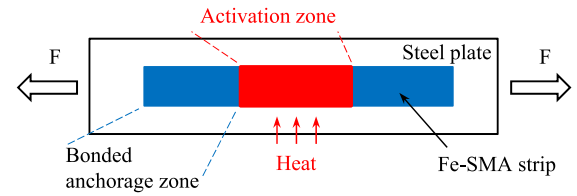
(a) A steel plate strengthened by Fe-SMA strips (both sides).
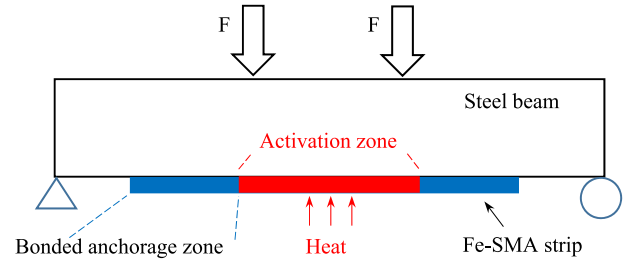
(b) A steel beam strengthened by an Fe-SMA strip.

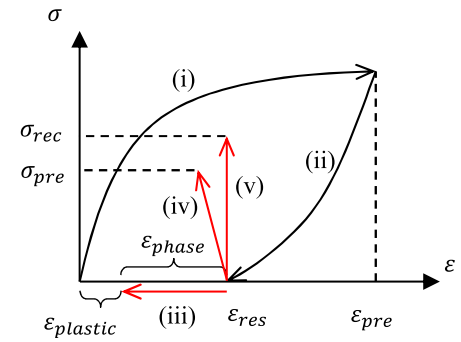**Fig. 1.** Schematic views of strengthening steel plates and beams.

Fig. 2. Schematic view of generating prestress. Red arrows refer to steps with heating. Paths (i) prestraining, (ii) unloading, (iii) heating with free deformation (no prestress), (iv) generating prestress with prestress loss, and (v) generating prestress without prestress loss. (For interpretation of the references to colour in this figure legend, the reader is referred to the web version of this article.)

portion ($\varepsilon_{plastic}$) [16,17]. (iii) Heating the unconstrained prestrained Fe-SMA leads to a shrinkage in the loading direction, as the phase transformation strain disappears due to a martensite to austenite phase transformation [18]; this is known as the shape memory effect. To utilize the shape memory effect for strengthening, (iv) the prestrained Fe-SMA strip is mounted to the target structure via mechanical or adhesive anchorages; the substrate restricts the shrinkage of the prestrained Fe-SMA strip when heated, resulting in a tensile stress in the Fe-SMA strip, which is known as the prestress (σ_{pre}). (v) If the prestrained Fe-SMA strip is fixed into a machine with a relatively infinite stiffness, the shrinkage of the Fe-SMA, when heated, is negligible, and the measured tensile stress is referred to as the recovery stress (σ_{rec}). It is worthy noting that the plastic strain does not contribute to the prestress generation. In seismic scenarios with Fe-SMAs exhibiting hysteresis and energy dissipation, both plastic and phase transformation strains play a role. For more details on the hysteresis behavior of Fe-SMAs, please refer to Refs. [19,20].

Several features, which influence the effectiveness of the bonded Fe-SMA strengthening with partial activation, have been identified through experimentation: a stronger prestressing effect can be achieved via (i) increasing the activation temperature within a certain range [11, 15], (ii) increasing the amount of Fe-SMA strips [11,21], and (iii) prolonging the bonded anchorage zone and activation zone simultaneously [21]. Simplified finite element (FE) models have succeeded in

analyzing the prestress level and deflection of steel [12] and glass [15] beams. Nevertheless, the impact of the aforementioned individual features on the prestress level in externally bonded Fe-SMA strengthening systems has not yet been quantified, posing challenges for engineers seeking to implement this strengthening technique.

Studying the efficacy of comparable prestressed strengthening techniques can enhance our understanding of bonded Fe-SMA strengthening. Externally bonded carbon fiber reinforced polymer (CFRP) strengthening [22–24] and embedded Fe-SMA strengthening [25–27] are closely related methods, as the former involves externally bonded strengthening, while the latter utilizes prestressed Fe-SMA. Although both techniques share similarities with the externally bonded Fe-SMA strengthening, significant differences still remain. The prestress of the externally bonded CFRP strengthening and the embedded Fe-SMA strengthening is typically generated along the entire CFRP and Fe-SMA strips/bars. However, in the case of externally bonded Fe-SMA strengthening, the prestress is generated only at the middle segment of the Fe-SMA strip, as shown in Fig. 1. As a result, the models constructed on the externally bonded CFRP strengthening and the embedded Fe-SMA strengthening cannot be directly applied to the externally bonded Fe-SMA strengthening case. It is, therefore, necessary to develop a suitable model that can accurately evaluate the prestressing effect of externally bonded Fe-SMA strengthening systems. Very recently, the authoring team investigated the behavior of the bonded anchorage zone and activation zone in Fig. 1, using Fe-SMA-to-steel adhesively bonded joints without [28,29] and with activation [30], respectively. This allows for a more precise analysis of the bonded strengthening system.

The present study aims to analyze the prestress level and deformation in steel, glass, and reinforced concrete (RC) structures strengthened by externally bonded/near surface mounted Fe-SMA strips/rebars. To accomplish this, two models, i.e., a symmetric strengthening model (illustrated in Fig. 1(a)) and an asymmetric strengthening model (illustrated in Fig. 1(b), later modified to Fig. A.13), are developed and validated using experimental results extracted from literature. A parametric study and a sensitivity analysis are conducted to assess the impact of the following features on the final prestress level: (i) the recovery stress level (equivalent to the activation temperature), (ii) the amount of Fe-SMA strips, and (iii) the prestress loss due to the compression of the substrates and shear deformation of bonded joints. Based on the findings, a design approach for utilizing the externally bonded/near surface mounted Fe-SMA strengthening solution is proposed. Finally, some perspectives on potential areas for future research are offered.

2. Prestressed strengthening models

In this section, a symmetric strengthening model and an asymmetric strengthening model are proposed, to analyze the effect of prestressed bonded Fe-SMA strengthening. Initially, the models are described for steel structures, and they will later be expanded to further include glass and RC structures.

2.1. Symmetric strengthening model

To strengthen a steel plate, Fe-SMA strips are typically bonded and activated symmetrically on both sides. Fig. 3 illustrates the free body diagram of half of a strengthened steel plate. To generate the prestress, Fe-SMA strips are typically heated to a temperature that is greater than 100 °C, which exceeds the glass transition temperature of many structural adhesives; therefore, the adhesive loses most of its stiffness and strength [31–33]. Thus, it is assumed that the adhesive in the activation zone is fully soft, i.e., eligible to shear deformation without bearing any shear stress. On the other hand, Li et al. [30] reported that, after an activation to a temperature of 180 or 260 °C and cooling to the room temperature, the bonded joint features a considerable shear capacity. This suggests that the adhesive re-cures

when the temperature returns to the room temperature. Experimental investigations [10,30,34] revealed a minimal temperature elevation in the bonded anchorage zone during activation, resulting in a negligible prestress induction in the Fe-SMA strip and a minimal change of adhesive properties. A swift temperature reduction was observed between the activation and bonded anchorage zones, as schematically illustrated in Fig. 3(d). By employing an electrical resistance heating, this temperature gradient zone spans less than 25 mm [30], which is short. Therefore, the temperature gradient zone is ignored in the current study.

Imagining a splitting of the Fe-SMA strips at the center line, the Fe-SMA strips tend to shrink during activation, as shown in Fig. 3(b). However, the activated Fe-SMA strips and substrate steel plate deform harmoniously in reality. Therefore, the steel plate and Fe-SMA strips are under compression and tension, respectively, as illustrated in Fig. 3(c). The equilibrium of Fig. 3(c) is expressed in terms of Eqs. (1)–(3)

$$2 \cdot F_{SMA} = F_{steel} \tag{1}$$

$$F_{SMA} = \sigma_{pre} \cdot A_{SMA} \tag{2}$$

$$F_{steel} = \sigma_{steel} \cdot A_{steel} \tag{3}$$

where F_{SMA} and F_{steel} represent the tensile and compressive forces in the Fe-SMA strip and steel plate, respectively; A_{SMA} and A_{steel} denote the cross-sectional areas of Fe-SMA strips on one side and the steel plate, respectively; σ_{pre} is the prestress held in the Fe-SMA, while σ_{steel} denotes the compressive stress in the steel plate, resulting from the generated prestress.

The generated prestress (σ_{pre}) can be computed as the recovery stress (σ_{rec}) subtracted by the prestress loss (σ_{loss}) (see Fig. 2). In this study, two major contributors to the prestress loss are considered, namely the compression of the steel plate (Δ_s) and the shear deformation of the adhesive joint (Δ_a), as illustrated in Fig. 3(c). Thus:

$$\sigma_{pre} = \sigma_{rec} - \sigma_{loss} \tag{4}$$

$$\sigma_{loss} = \frac{\Delta_s + \Delta_a}{L_{act}} \cdot E_{SMA} \tag{5}$$

$$\sigma_{steel} = \frac{\Delta_s}{L_{act}} \cdot E_{steel} \tag{6}$$

where L_{act} means half of the activation length; E_{steel} denotes the E-modulus of the steel plate; E_{SMA} represents the secant modulus (rather than the elastic modulus) of the Fe-SMA strip in the quasi-linear stage, as illustrated in Fig. 4. The secant modulus (E_{SMA}) is characterized by primarily an elastic deformation accompanied by a phase transformation. The prestress loss is attributed to unloading of the Fe-SMA strip, which contains primarily an elastic deformation accompanied by a phase transformation. The secant moduli, denoted as secant (i) in Fig. 4 and measured between 20 MPa and 300 MPa, are 153.3 GPa and 137.5 GPa for non-prestrained and prestrained Fe-SMA strips, respectively [28]. These values closely align with the unloading modulus of approximately 150 GPa for Fe-SMA strips prestrained to 2% [35], identified by secant (ii) in Fig. 4 and characterized between 600 MPa and 300 MPa. Additionally, an experimental study delivered by Izadi et al. [36] determined a modulus of approximately 140 GPa for the prestress loss, represented as secant (iii) in Fig. 4. These moduli fall within the same range, confirming the adequacy of utilizing the secant modulus (E_{SMA}) for analyzing the prestress loss.

Substituting Eqs. (2)–(6) into Eq. (1) yields Eq. (7).

$$\Delta_s = \frac{2 \cdot \sigma_{rec} \cdot L_{act} \cdot A_{SMA} - 2 \cdot \Delta_a \cdot E_{SMA} \cdot A_{SMA}}{E_{steel} \cdot A_{steel} + 2 \cdot E_{SMA} \cdot A_{SMA}} \tag{7}$$

In the meantime, the tensile force in the Fe-SMA strip is balanced by the shear force at the bonded joint, which can be expressed in terms of Eq. (8). Substituting Eqs. (2), (4) and (5) into Eq. (8) yields Eq. (9).
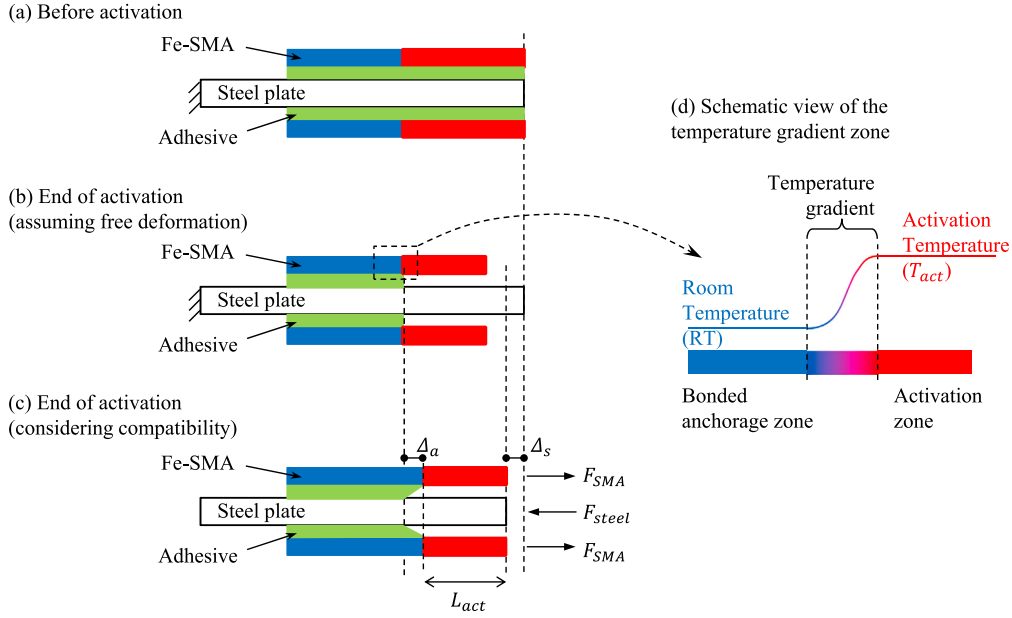
$$F_{SMA} = f_{F-\Delta}(\Delta_a) \tag{8}$$

(a) Before activation

(d) Schematic view of the temperature gradient zone

(b) End of activation (assuming free deformation)

(c) End of activation (considering compatibility)

Fig. 3. Schematic view of a strengthened steel plate with bonded Fe-SMA strips, only half of the symmetric system is shown.
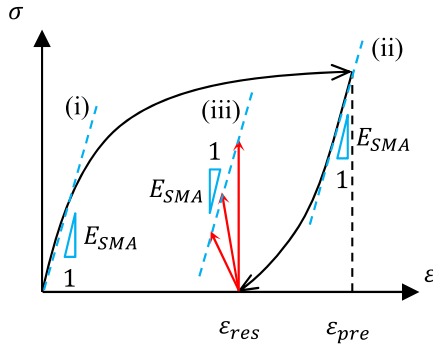

Fig. 4. Schematic of the secant modulus (E_{SMA}) for estimating prestress loss. Red arrows refer to generating prestress with different substrate stiffnesses. Secants (i-iii) are: (i) loading secant modulus, (ii) unloading secant modulus, (iii) modulus for estimating prestress loss (σ_{loss}). (For interpretation of the references to colour in this figure legend, the reader is referred to the web version of this article.)

$$\left(\sigma_{rec} - \frac{\Delta_s + \Delta_a}{L_{act}} \cdot E_{SMA} \right) \cdot A_{SMA} = f_{F-\Delta}(\Delta_a) \tag{9}$$

where $f_{F-\Delta}(\cdot)$ represents the load–displacement curve of the adhesively bonded joint, which is depicted in Fig. 5. It can either be measured via a lap-shear test [28] or computed by a model [29] with a given bond–slip behavior.

Solving Eqs. (7) and (9) via numerical iterations leads to the final results, including the prestress loss, retained prestress level in the strengthening system, and deformations of the steel plate and adhesive joint. In Eqs. (8) and (9), the full load–displacement curve of the bonded anchorage zone with an arbitrary bond length is utilized, which characterizes a nonlinear behavior. In the case of localized strengthening, where the bond length is rather short, the nonlinear stage of the load–displacement behavior could be utilized (the dashed blue curve in Fig. 5). On the other hand, if the bond length is long, as in the case of strengthening for a steel girder, which will be introduced in the next section, only the quasi-linear stage of the load–displacement behavior is utilized (the solid black curve in Fig. 5), and Eqs. (8) and (9) can be approximated by a closed-form solution.

2.2. Asymmetric strengthening model

To strengthen a steel beam, the Fe-SMA strip is preferably bonded on the tensile side, as illustrated in Figs. 1(b) and 6. After activation of the Fe-SMA strip, the generated prestressing force induces a compressive stress field, countering the external load-induced deformation and alleviating the tensile stress, thus boosting the fatigue, stability and flexural performance of the steel beam. Applying again the assumption of a fully softened adhesive in the activation zone during the activation process, the equilibrium can be analyzed based on Fig. 6(c). The activation segment is further analyzed via Fig. 7.

Simplifying the activation zone into a segment with a length of $2 \cdot L_{act}$, which is eccentrically loaded, as demonstrated in Fig. 7(a), it is equivalent to a segment loaded by a compress force passing through the axis and a bending moment, as illustrated in Fig. 7(b). The axial force and bending moment read Eqs. (10) and (11), respectively. Targeting global strengthening, the Fe-SMA strip is required to be sufficiently long, leading to a high ratio of the activation length over beam height ($2 \cdot L_{act}/h$). As a result, the condition for an Euler–Bernoulli beam applies, and the compressive and bending strains at the edge of height read Eqs. (12) and (13), respectively.

$$F = \sigma_{pre} \cdot A_{SMA} \tag{10}$$

$$M = \sigma_{pre} \cdot A_{SMA} \cdot \frac{h}{2} \tag{11}$$

$$\varepsilon_{comp} = \frac{\sigma_{pre} \cdot A_{SMA}}{A_{steel} \cdot E_{steel}} \tag{12}$$

$$\varepsilon_{bending} = \frac{\sigma_{pre} \cdot A_{SMA} \cdot h^2}{4 \cdot I \cdot E_{steel}} \tag{13}$$

where F and M are the prestressing force and corresponding moment in the activation segment, respectively, applied at the middle of beam height; A_{SMA} and A_{steel} refer to cross-sectional areas of the Fe-SMA strip and steel beam, respectively; h and I are the height and moment of inertia of the beam, respectively; ε_{comp} and $\varepsilon_{bending}$ represent strain components due to compression and bending, respectively, at the edge of height in the activation segment; E_{steel} means the E-modulus of the steel beam.
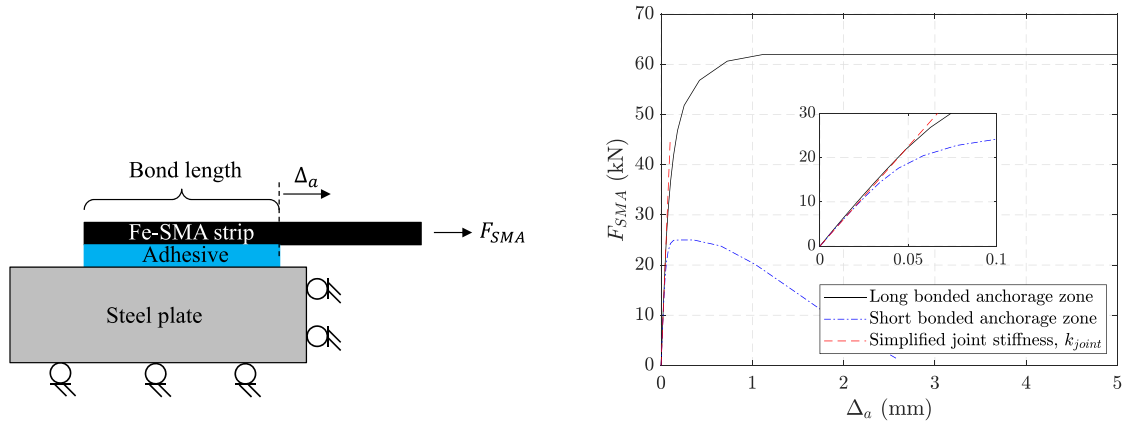
(a) Scheme of a Fe-SMA lap-shear joint, where F_{SMA} represents the tensile load and Δ_a denotes the shear deformation of the adhesive joint.

(b) Load-displacement curves of Fe-SMA lap-shear joints with varying bond lengths, computed by a model [29] with a given bond-slip behaviour.

Fig. 5. Load–displacement behaviors of bonded anchorage zones with different bond lengths. The Fe-SMA strip has a width of 50 mm and a thickness of 1.5 mm. (For interpretation of the references to colour in this figure legend, the reader is referred to the web version of this article.)
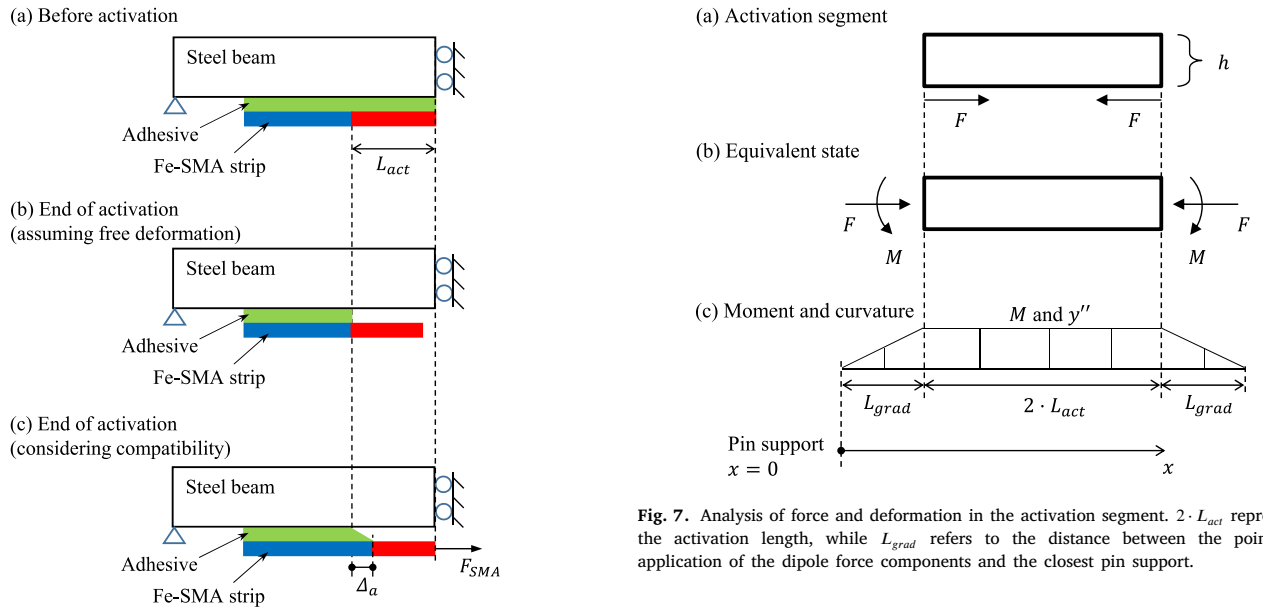

Fig. 6. Schematic view of a strengthened steel beam with a bonded Fe-SMA strip, only half of the symmetric system is shown.

Fig. 7. Analysis of force and deformation in the activation segment. $2 \cdot L_{act}$ represents the activation length, while L_{grad} refers to the distance between the points of application of the dipole force components and the closest pin support.

$$\Delta_a = \frac{F}{k_{joint}} = \frac{\sigma_{pre} \cdot A_{SMA}}{k_{joint}} \tag{15}$$

$$\sigma_{pre} = \frac{\sigma_{rec}}{1 + \underbrace{\frac{A_{SMA} \cdot E_{SMA}}{A_{steel} \cdot E_{steel}}}_{\text{compression term}} + \underbrace{\frac{A_{SMA} \cdot E_{SMA} \cdot h^2}{4 \cdot I \cdot E_{steel}}}_{\text{bending term}} + \underbrace{\frac{A_{SMA} \cdot E_{SMA}}{L_{act} \cdot k_{joint}}}_{\text{joint slip term}}} \tag{16}$$

where σ_{loss} means the prestress loss; k_{joint} and Δ_a represent the loading stiffness and shear deformation of the adhesive joint, respectively.

Furthermore, the deflection of the steel beam due to the applied prestressed strengthening has a closed-form solution as well. The bending moment keeps a constant in the activation segment of the beam, outside which the bending moment linearly decreases until the pin support, as shown in Fig. 7(c). The bending stress and strain at the edge of an arbitrary cross-section at x_i reads Eqs. (17) and (18), which lead to the second order derivative of deflection (curvature), as written per Eq. (19).

Apart from the prestress loss due to the shear deformation of the adhesive joint and the compressive deformation of the beam, the bending deformation further reduces the length of the edge. As a result, the prestress loss, similar to that in the symmetric strengthening model, is expressed as Eq. (14). In the case of strengthening of an Euler–Bernoulli beam, the lengths of the activation zone and bonded anchorage zone can be efficiently long, leading to a satisfactory bond capacity. As a result, the ratio of the prestressing force over the bond capacity remains low. Therefore, only the quasi-linear stage of the load–displacement behavior of the adhesive joint is exploited, which can be simplified as the red dashed line in Fig. 5, and the shear deformation of the adhesive joint can be computed as Eq. (15). Substituting Eqs. (12) to (15) into Eq. (4) yields an explicit solution of the prestress level, which reads Eq. (16).

$$\sigma_{loss} = \left(\varepsilon_{comp} + \varepsilon_{bending} + \frac{\Delta_a}{L_{act}} \right) \cdot E_{SMA} \tag{14}$$

$$\sigma_{bending,i} = \frac{M_i}{I} \cdot \frac{h}{2} = \frac{E \cdot I \cdot y_i''}{I} \cdot \frac{h}{2} \tag{17}$$

Table 1
Summarization of collected tests.

Groupno.	Parentstructure	Position of bonded Fe-SMA strips/rebars	Activation techniques	Activation temperature (°C)	Analysis model
(1)	Steel plates [11,21]	Both sides of plates	Electricity	120, 180, and 260	Symmetric model
(2)	Glass plates [14]	Top and bottom edges	Electricity	160	Symmetric model
(3)	Steel beams [12,13]	Bottom flanges	Flame	140 and 240	Asymmetric model
(4)	Glass beams [15]	Bottom edges	Electricity	120, 140, and 160	Asymmetric model
(5)	RC beams [37]	Top layer	Electricity	192 and 200	Modified asymmetric model

$$\varepsilon_{bending,i} = \frac{h}{2} \cdot y_i'' \tag{18}$$

$$y_i'' = \frac{2 \cdot \varepsilon_{bending,i}}{h} \tag{19}$$

where y means the deflection of the beam; M_i and y_i'' represent the bending moment and curvature at an arbitrary cross-section of the beam, while $\varepsilon_{bending,i}$ refers to as the bending strain at the edge of this arbitrary cross-section.

Due to symmetry, only the left half of Fig. 7(c), which is supported by $x = [0, L_{grad} + L_{act}]$, is analyzed. The curvature of the left half of the beam reads Eq. (20).

$$y''(x) = \begin{cases} \frac{2 \cdot \varepsilon_{bending}}{h \cdot L_{grad}} \cdot x, \text{if } 0 \leq x \leq L_{grad} \\ \frac{2 \cdot \varepsilon_{bending}}{h}, \text{if } L_{grad} < x \leq L_{grad} + L_{act} \end{cases} \tag{20}$$

where L_{grad} represents the distance between the points of application of the dipole force components and the closest pin support; L_{act} corresponds to half of the activation length; $\varepsilon_{bending}$ is identical to that in Eq. (13).

Conducting twice integral, with adopting boundary conditions as expressed in terms of Eq. (21), the deflection at the mid-span reads Eq. (22).

$$y|_{x=0} = 0$$
$$y'|_{x=L_{grad}+L_{act}} = 0 \tag{21}$$

$$y|_{x=L_{grad}+L_{act}} = -\frac{\varepsilon_{bending}}{h} \cdot \left(\frac{2}{3} \cdot L_{grad}^2 + 2 \cdot L_{grad} \cdot L_{act} + L_{act}^2 \right) \tag{22}$$

where a negative value suggests an upward deflection.

It is worth noting that an Euler–Bernoulli beam is assumed in this model, which requires a high aspect ratio ($2 \cdot L_{act}/h$). It corresponds to the strengthening for the global loading and deformation behaviors. However, in the case of locally bonded strengthening using Fe-SMA strips (low $2 \cdot L_{act}/h$), an analytical solution employing the Timoshenko beam theory or a numerical solution may be required, which is beyond the scope of the current study.

3. Experiments for validation of the proposed models

Several experimental studies [11–15,21,37] employed bonded Fe-SMA strips/rebars to improve the performance of steel, glass, and RC structural members. Prior to mechanical tests, Fe-SMA strips/rebars were heated to generate prestress; this procedure is known as the activation test, during which strains and deformations of substrate members were measured to analyze the prestress level. According to the types of parent structures, five groups, as listed in Table 1, are categorized in the current study: (1) steel plates [11,21], (2) glass plates [14], (3) steel beams [12,13], (4) glass beams [15], and (5) RC beams [37]. The measured strains and deflections at the midline of plates or mid-span of beams during activation tests are used to validate the two proposed models. Strengthening details of these five groups, including the geometry, activation temperature, and generated recovery stress, are listed in Tables 2 to 4.

3.1. Group (1): strengthening steel plates

Some authors of the current study [11,21] used bonded Fe-SMA strips to strengthen steel plates with central through-thickness cracks, aiming to prolong the fatigue life or arrest the growth of existing cracks. Prior to the fatigue tests, prestress was generated symmetrically via electrical resistance heating, during which the compressive strain in the midline of steel plates was measured via strain gauges. An adhesive, SikaPower 1277, was employed to bond Fe-SMA strips symmetrically onto two sides of steel plates. The thickness of the adhesive layer was controlled at ca. 0.5 mm. The load–displacement behavior of Fe-SMA-to-steel lap-shear joints [28,29], comprising the same adhesive and Fe-SMA strip, is utilized to analyze the prestress loss due to the adhesive joint deformation (Eq. (8)). The activation details for ten strengthened steel plates are listed in Table 2. The symmetric strengthening model is applied.

3.2. Group (2): strengthening glass plates

Silvestru et al. [14] utilized bonded Fe-SMA strips to strengthen glass beams to enhance their load carrying capacity and ductility. The strengthening was applied on both the upper and lower edges of glass beams and activation was conducted via electrical resistance heating, applied simultaneously and symmetrically. Despite the loading configuration of four-point bending during the mechanical test, the resultant prestressing force went through the axis of the narrow glass beams during the activation test. Therefore, these glass beams are regarded as glass plates during the activation tests, and the symmetric strengthening model applies. The adhesive used was SikaPower 1277, with a thickness of ca. 1.5 mm. Since the authors of the current study have no data for bond behavior of this adhesive thickness, an average loading stiffness of Fe-SMA-to-steel lap-shear joints with adhesive thicknesses of 1 and 2 mm [28] is employed to estimate the amount of prestress loss caused by the adhesive joint. Activation details of three strengthened glass plates are detailed in Table 2.

3.3. Group (3): strengthening steel beams

Part of the current authoring team [12,13] conducted feasibility investigations on the strengthening of steel beams via use of partly and fully bonded Fe-SMA strips. The prestress was activated via flame heating. Since the adhesive layer held a substantially reduced stiffness during the activation, its stiffness is assumed to be null in the model. Therefore, the difference between partly and fully bonded strengthening schemes is ignored during the prestress analysis. Moreover, the Fe-SMA strips were bonded only at the bottom flanges, with the generated prestress resulting in bending, thus requiring an asymmetric strengthening assumption. The employed adhesive once again was SikaPower 1277 with an approximate thickness of 0.5 mm, whose loading stiffness was reported by Li et al. [28]. Details of the activation tests of two strengthened steel beams are listed in Table 3.

Table 2
Details of strengthened steel and glass plates, groups (1 and 2).

	Specimen symbol[a]	L_{anchor} (mm)	L_{act} (mm)	T_{act} (°C)	σ_{rec} (MPa)	A_{SMA} (mm^2)	A_{sub}[b] (mm^2)
Steel plates [21]	S-100	25	25	120[c]	230	75	1500
	SC-100	25	25	180	320	75	1500
	SC-200	50	50	180	320	75	1500
	S-300	75	75	180	320	75	1500
	SC-300	75	75	180	320	75	1500
	SC-500	125	125	180	320	75	1500
Steel plates [11]	SP-Act120	150	100	120	230	150	1500
	SP-Act180	150	100	180	320	150	1500
	SP-Act260-1	150	100	260	400	150	1500
	SP-Act260-2	150	100	260	400	150	1500
Glass plates [14]	BT-10-SP-a	325	425	160	300	37.5	2684
	BT-11-SP-a	325	425	160	300	37.5	2684
	BT-12-SP-a	325	425	160	300	37.5	2684

E_{SMA} = 153 GPa; E_{steel} = 200 GPa; E_{glass} = 70 GPa.
[a] Specimen symbols are identical to those in the references.
[b] A_{sub} refers to the cross-sectional area of substrate plates, including A_{steel} for steel plates and A_{glass} for glass plates.
[c] The target activation temperature was 180 °C, however, four thermocouples reported an average value of ca. 120 °C.

Table 3
Details of strengthened steel and glass beams, groups (3 and 4).

	Specimen symbol[a]	L_{grad} (mm)	L_{act} (mm)	T_{act} (°C)	σ_{rec} (MPa)	A_{SMA} (mm^2)	A_{sub}[b] (mm^2)	h (mm)	I (mm^4)
Steel beams [12,13]	SB-part	790	1860	240[c]	324[d]	1500	6870	300	97,180,000
	SB-full	790	1860	140	283[d]	1500	6870	300	97,180,000
Glass beams [15]	P_T120-I	350	350	122	201.7[d]	15	1200	100	951,294
	P_T120-II	350	350	124	207.0[d]	15	1200	100	951,294
	P_T140	350	350	142	263.8[d]	15	1200	100	951,294
	P_T160	350	350	161	355.2[d]	15	1200	100	951,294

E_{SMA} = 153 GPa; E_{steel} = 200 GPa; E_{glass} = 74 GPa.
[a] SB-part and SB-full represent steel beams strengthened by partly bonded and fully bonded strategies, respectively. The remaining specimen symbols are identical to those in the references.
[b] A_{sub} refers to the cross-sectional area of substrate beams, including A_{steel} for steel beams and A_{glass} for glass beams.
[c] The entire unbonded region and a part of the bonded region were heated to 240 and 140 °C, respectively.
[d] Values of σ_{rec} reported in respective studies.

3.4. Group (4): strengthening glass beams

Rocha et al. [15] strengthened glass beams via bonding Fe-SMA strips at the bottom edges. The prestress was activated via electrical resistance heating. Due to the eccentrically applied strengthening, where a bending effect is pronounced, the asymmetric strengthening model applies. Different from the previous three groups, the adhesive 3 M Scotch-Weld DP490, with an approximate thickness of 0.3 mm, was utilized in this group, whose bond behavior is unavailable to the authors of the current study. Nevertheless, this adhesive share similar properties to SikaPower 1277. Studies on CFRP bonded joints [38–40] revealed that similar adhesive properties lead to alike bond behaviors. Therefore, the stiffness of adhesive joints in this group is assumed identical to that of Fe-SMA-to-steel joints comprising SikaPower 1277 with a joint thickness of 0.5 mm. Details of activation tests of four strengthened glass beams are listed in Table 3.

3.5. Group (5): strengthening RC beams

Schranz et al. [37] strengthened RC beams via embedding Fe-SMA rebars to the top of RC beams by cementitious mortar. Two techniques, cover replacement (CR) and near surface mounting (NSM), were employed for strengthening. The prestress was activated again via electrical resistance heating. The loading stiffness of the Fe-SMA-to-mortar joints, for analyzing the prestress loss due to the Fe-SMA rebar slip, is calculated employing a model proposed by Li et al. [29]. The specimen geometry and boundary conditions in this group are different from those in the symmetric and asymmetric strengthening models. Therefore, the asymmetric strengthening model is modified, whose derivation is presented in Appendix A, to predict the strengthening

behavior. Details of activation tests of two strengthened RC beams are presented in Table 4.

4. Validation on experimental data

Adopting the symmetric, asymmetric, and modified asymmetric strengthening models, along with activation details listed in Tables 2 to 4, strains and deflections of the parent structures, as well as the retained prestress levels, can be easily computed. All Fe-SMA strips with a thickness of 1.5 mm were manufactured by re-fer AG (Switzerland). They were prestrained to ca. 2% [11–15,21]. Therefore, a consistent Fe-SMA behavior is assumed for all Fe-SMA strips in the following analysis. For specimens with a special activation process or with the prestress back-calculated via an FE simulation, the recovery stress (σ_{rec}) values reported in respective studies are adopted in our analysis. Otherwise, the following recovery stress values, with activation temperatures in parentheses, are employed: 230 MPa (120 °C), 300 MPa (160 °C), 320 MPa (180 °C), and 400 MPa (260 °C) [6,7,36,41]. It is noteworthy that the thermal expansion of the substrates would have reduced the generated recovery stress to some extent, given an experimental observation that the elongation of the substrate reduces the recovery stress [4]. However, the thermal expansion due to the local temperature elevation in the substrates is magnitudes lower than that reported in Ref. [4]. Therefore, such a reduction of the generated recovery stress is insignificant and ignored in the analysis. Fig. 8 demonstrates a comparison between the predicted strains and deflections and their corresponding experimental measurements. The values of strains and deflections are presented in Table B.7 in Appendix B.

Table 4
Details of strengthened RC beams, group 5 [37].

Specimen symbol[a]	L_1 (mm)	L_2 (mm)	T_{act} (°C)	σ_{rec} (MPa)	E_c (GPa)	A_{SMA}[b] (mm²)	A_{SMA}^*[c] (mm²)	A_c (mm²)	h (mm)	I (mm⁴)
2-CR-act	2400	2400	200	340[d]	38.5	565	113	216,000	216	848,500,000
4-NSM-act	2400	2400	192	330[d]	39.0	565	113	230,000	230	965,400,000

[a] Specimen symbols are identical to those in the reference.
[b] A_{SMA} refers to the total cross-sectional area of strengthening Fe-SMA rebars.
[c] A_{SMA}^* stands for the cross-sectional area of a single Fe-SMA rebar.
[d] Values of σ_{rec} are linearly interpolated between activation temperatures of 180 and 260 °C.
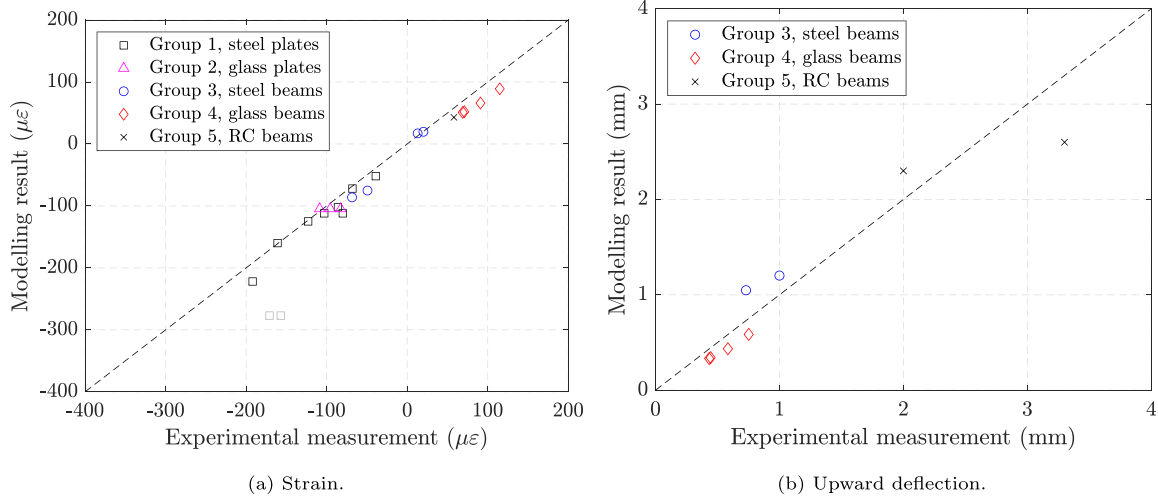

(a) Strain. (b) Upward deflection.

Fig. 8. Model prediction vs. experimental measurement in terms of strain and deformation.

4.1. Strains

Fig. 8(a) exhibits that, apart from the two gray squares, strain predictions closely approximate the experimental measurements, albeit with certain deviations. These deviations can be attributed to the simplifications adopted in the symmetric and asymmetric strengthening models, the uncertainty in the measured recovery stress, and the measurement error of strains. As mentioned in the model assumptions, a temperature gradient zone is situated between the activation zone and bonded anchorage zone, to accommodate the temperature gradient from the activation temperature down to the room temperature. Despite its short length, Fe-SMA strips there are expected to have undergone some level of prestressing, while the adhesive layer should have experienced a reduction in stiffness due to heating. The two proposed models, which ignore the temperature gradient zone, adopt a fully soft adhesive bond in the activation zone and an unaffected adhesive bond in the bonded anchorage zone. Such a simplification introduces some level of error.

Additionally, uncertainty of the recovery stress affects the analysis at two distinct levels. Firstly, Fe-SMA strips, which are produced by re-fer AG and subject to an identical prestrain level and activation temperature, may exhibit some deviation of the measured recovery stress values [6,7,36,41]. To account for this, an intermediate value among collected recovery stress values at each activation temperature is adopted in our model analysis. Secondly, during the activation process, different locations on the same Fe-SMA strip may experience variations in activation temperature [12–14,21,30], leading to further deviations of the generated recovery stress. Due to the aforementioned facts, predicting the value of the generated recovery stress proves challenging, resulting in uncertainties when calculating the prestress level and later deformation of structural members.

Furthermore, when considering local strengthening with a short activation zone, such as S-100 and SC-100 in Ref. [21], it is important

to note that the compression of the substrate induced by the prestressing force is not uniformly distributed across the entire cross-section. Instead, it exhibits a gradient. Although the average strain measured by several strain gauges can provide an estimation of this gradient, there may still be some degree of error involved.

The two gray squares in Fig. 8(a) represent two steel plates strengthened by bonded Fe-SMA strips, which were heated to an activation temperature of 260 °C. During the activation process, the temperature of the steel plates was raised to 110−120 °C, which exceeds the temperature range (up to 100 °C) of the strain gauges employed, leading to inaccurate strain measurement. Nevertheless, the experimentally observed phenomenon of arresting the crack growth at certain load levels [11] confirms the accuracy of strains computed by our model. The remaining strain measurements are deemed reliable. This is because the remaining strain gauges were positioned either near the activation zone, where the elevated temperature during measurements stayed within the specified temperature range for the gauges, or on the flange/edge opposite the activation side, where the activation temperature had no impact.

4.2. Deflections

Fig. 8(b) demonstrates that the predicted deflections of steel, glass, and RC beams fairly well approximate the experimental measurements. The deflections of the steel beams are consistently slightly overestimated, while those of glass beams are consistently slightly underestimated. The errors of RC beam deflection seem to be random. Such a tendency could be attributed to the activation strategy. Steel beams were activated via flame heating [12,13], which required long heating time; more energy entered the system, leading to an expansion of the aforementioned temperature gradient zone and unexpected softening of adhesive at the bonded anchorage zone. This results in extra prestress loss, and it is in line with the slightly overestimated strain in the steel
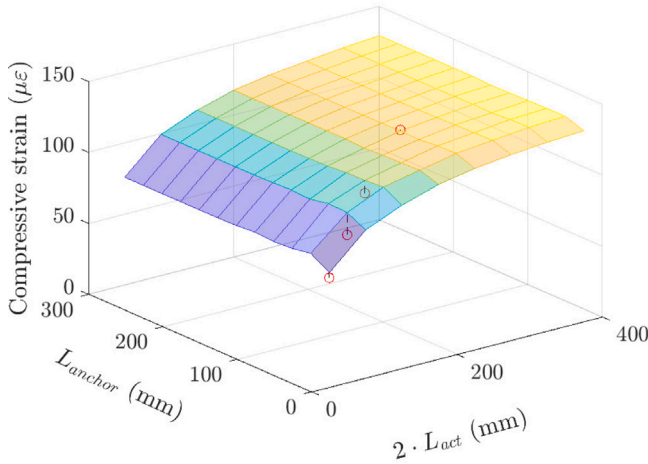
Fig. 9. Effect of the bonded anchorage length (L_{anchor}) and activation length ($2 \cdot L_{act}$), while the Fe-SMA strip width (b_{SMA}) and recovery stress level (σ_{rec}) are kept constant. The red dots are experimentally measured strains [21].

beams. On the other hand, the glass beams were activated via electrical resistance heating [14,15], which required shorter heating time. However, the elevated temperature at the edges of glass beams could have reduced the stiffness there, due to a temperature dependency of the glass members [42,43]. Such a reduced stiffness resulted in higher deflection. As a result, the measured deflections and strain of glass beams are slightly larger than those computed. A second source of error could be attributed to the assumed shear stiffness of adhesive joints comprising the adhesive 3 M Scotch-Weld DP490 with a thickness of 0.3 mm, which is represented by that of a similar adhesive SikaPower 1277 with a thickness of 0.5 mm. The third source of the deflection error could be the simplified Euler–Bernoulli beam, with which the local deformation due to the concentrated di-pole force is ignored. Since the deformations incurred by the prestress remain at a low level (less than 2 mm), such a local deformation could play a role.

Although some discrepancies exist between the model prediction and experimental measurements, the proposed models have demonstrated a fairly accurate ability to predict the prestress level and deflection of steel, glass, and RC members strengthened by externally bonded/near surface mounted Fe-SMAs. To enhance the accuracy of the models, further investigation is needed to (i) assess the impact of the aforementioned temperature gradient zone and (ii) quantify the uncertainties in the recovery stress.

5. Influence of each variable on the prestressing effect

After a successful validation of the proposed models, it is worth quantifying the influence of each variable on the final prestress level, which offers a guidance to the engineering design. Four influential variables are characterized: (i) the bonded anchorage length (L_{anchor}), (ii) the activation length (L_{act}), (iii) the Fe-SMA strip width (b_{SMA}), and (iv) the recovery stress (σ_{rec}, equivalent to the activation temperature, T_{act}). The symmetric strengthening model is employed in this section. Fig. 9 exhibits a combined effect of the bonded anchorage length and activation length, while the Fe-SMA strip width and recovery stress are kept constant. It is clearly seen that increasing the bonded anchorage length and activation length enhances the prestressing effect, in terms of the compressive strain in the steel plate. The red dots, which are experimentally measured strains [21], further confirm this conclusion and verify the feasibility of a parametric study.

5.1. Parametric study

The influence of the four previously described characteristic variables are visualized in Fig. 10. Figs. 10(a) and 10(b), which are projections of Fig. 9 on different planes, demonstrate the influence of the bonded anchorage length and activation length, respectively. Fig. 10(a) shows that the bonded anchorage length saturates very soon. A further extension of the anchorage length does not further increase the prestressing effect. The reason is that the loading stiffness (Eq. (8)) and the load transferring capacity (bond capacity) of a short bonded anchorage zone remain low, and a lower loading stiffness leads to greater prestress loss (Eqs. (5), (8) and (15)). Any increase in the bonded anchorage length can effectively enhance the loading stiffness, thus, leading to a reduced prestress loss and an improved prestress level. However, such a loading stiffness saturates at an approximate anchorage length of $L_{anchor} = 50$ mm. Afterwards, prolonging the bonded anchorage length enhances the bond capacity while maintaining the loading stiffness. Note, the effective bond length of the joints employed is approximately 138 mm [28], over which the bond capacity does not further increase; the threshold anchorage length of 50 mm is ca. 1/3 of the effective bond length.

Fig. 10(b) shows that the prestress level, in terms of compressive strain of the substrate, increases with the activation length, and the increment of the prestress level reduces with the activation length. Substituting Eq. (7) into Eq. (5) yields Eq. (23), in which only Δ_a and L_{act} are variables, while the rest are constant. As explained in the previous paragraph, when the bonded anchorage length saturates, the loading stiffness does not change any more, leading to a constant deformation of the adhesive joint (Δ_a). Therefore, an increasing activation length (L_{act}) leads to a reduced prestress loss and an enhanced prestress level. The increment of the prestress level reduces as the activation zone becomes longer. The maximum prestress level that a strengthening system can reach is expressed in terms of Eq. (25) (substituting Eq. (23) into Eq. (4)); when the activation length becomes infinite large, the prestress loss due to the deformation of the bonded anchorage zone (Δ_a) is negligible. This prestress level is persistently less than the generated recovery stress, due to the prestress loss resulting from the compression of the substrate member. To further increase the prestress level, a higher activation temperature with a greater recovery stress is required. The three curves in Fig. 10(b), with the bonded anchorage lengths over the threshold of $L_{anchor} = 50$ mm, experience negligible difference.

$$\sigma_{loss} = \underbrace{\sigma_{rec} \cdot \rho}_{constant} + \underbrace{\frac{\Delta_a}{L_{act}}}_{varying} \cdot \underbrace{E_{SMA} \cdot (1 - \rho)}_{positive\ constant} \quad (23)$$

$$\rho = \frac{2 \cdot E_{SMA} \cdot A_{SMA}}{E_{steel} \cdot A_{steel} + 2 \cdot E_{SMA} \cdot A_{SMA}} \quad (24)$$

$$\lim_{L_{act} \to \infty} \sigma_{pre}(L_{act}) = \sigma_{rec} \cdot (1 - \rho) \quad (25)$$

where ρ refers to as the stiffness ratio of the bonded Fe-SMA strengthening system.

Figs. 10(c) and 10(d) exhibit that increasing either the recovery stress (equivalent to the activation temperature) or the Fe-SMA strip width leads to an enhanced prestressing effect, in terms of the compressive strain in the steel plate. The inherent reason is straightforward. A higher recovery stress level with an unchanged cross-section leads to a higher prestressing force, resulting in a stronger prestressing effect. So does a wider cross-section with an unchanged recovery stress level. The recovery stress is, at the moment, limited by the Fe-SMA itself. The Fe-SMA used in the current study has a recovery stress of ca. 400 MPa at a prestrain level of 2% and an activation temperature of 260 °C. Further increasing the prestrain level or activation temperature cannot substantially enhance the prestress level [7,41]. An even higher activation temperature may bring adverse effects to the adhesive layer, such as heating damage [30].
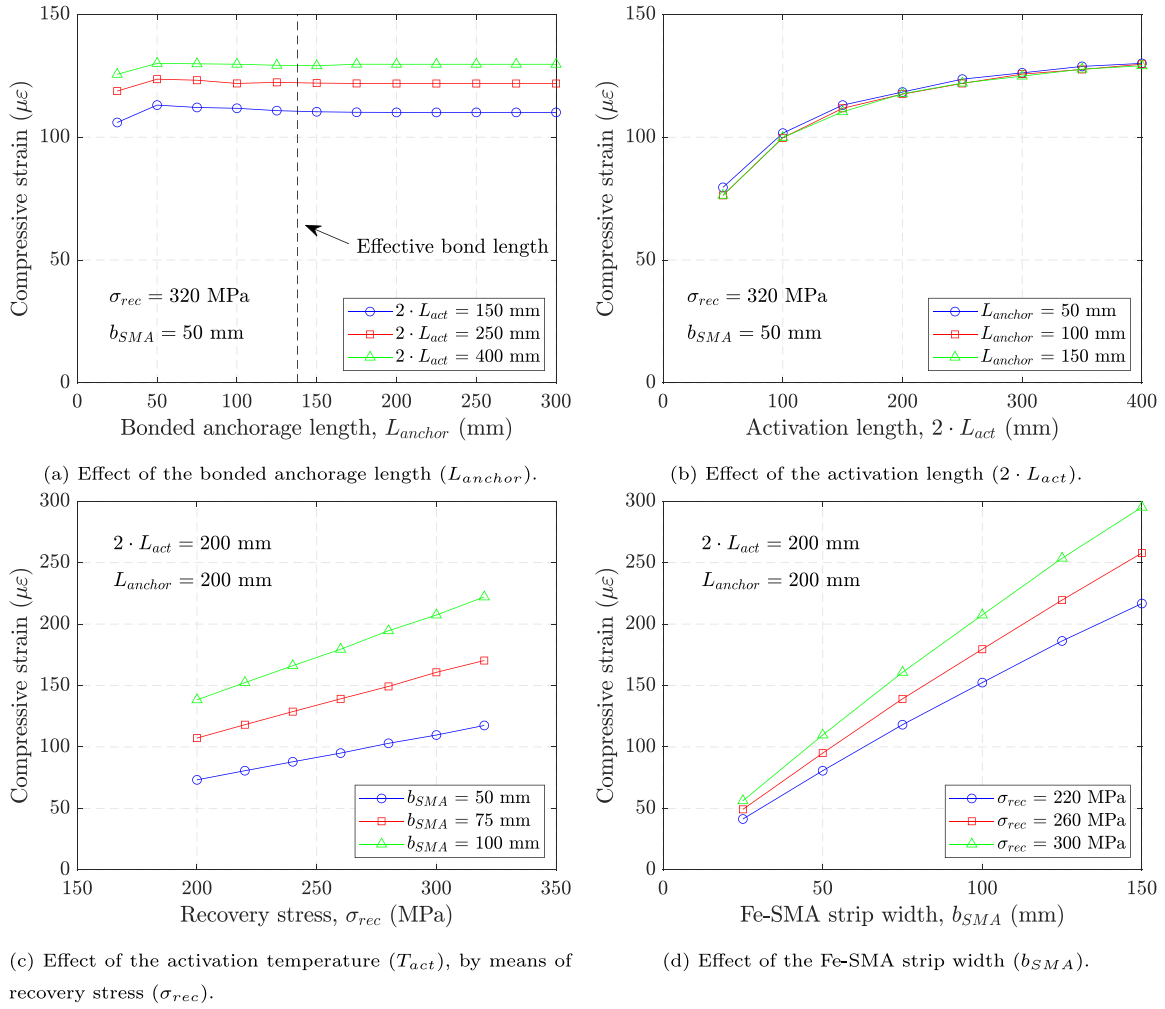
(a) Effect of the bonded anchorage length (L_{anchor}).

(b) Effect of the activation length ($2 \cdot L_{act}$).

(c) Effect of the activation temperature (T_{act}), by means of recovery stress (σ_{rec}).

(d) Effect of the Fe-SMA strip width (b_{SMA}).

Fig. 10. The effect of influential features. The substrate steel plate has a width of 150 mm and a thickness of 10 mm, identical to Refs. [11,21], while the Fe-SMA strip has a thickness of 1.5 mm.

On the other hand, the Fe-SMA strip width, which is limited by the space, can ultimately reach the width of the substrate steel plate. If the Fe-SMA strip width saturates, one could consider to increase the Fe-SMA strip thickness. Prior to the prestress loss, the prestressing force proportionally increases with the strip thickness. However, the effect of the Fe-SMA strip thickness on the bond behavior remains unclear at the moment. Eq. (26) derived from CFRP bonded joints [38,44–46] indicates that the bond capacity increases proportionally to the square root of the strips thickness. Therefore, it is expected that increasing the Fe-SMA strip thickness enhances the prestressing effect, meanwhile, it brings a chance of premature debonding failure, since the increase of bond capacity is slower than the prestressing force. More investigation on Fe-SMA bond is required in this regard.

$$F_b = b_f \cdot \sqrt{2 \cdot E_f \cdot t_f \cdot G_f} \qquad (26)$$

where F_b represents the bond capacity; E_f, b_f, and t_f represent the E-modulus, width, and thickness of the CFRP strip, respectively; G_f means the fracture energy of the bond line.

Based on this parametric study, which is visualized in Fig. 10, the following can be deduced. The bonded anchorage length bears the lowest influence on the variation of the prestressing effect. However, a minimum bonded anchorage zone, which holds the prestressing force, should be guaranteed. Otherwise, the strengthening system would fail during the activation process [30]. Increasing the other three variables can substantially enhance the prestress effect, with certain caps: (i) enhancing the activation length is capped by the recovery stress level;

(ii) increasing the recovery stress via elevating the activation temperature is limited by the Fe-SMA material and the underneath adhesive; (iii) adding the width of Fe-SMA strips is limited by the space. Their importance is further quantified by a sensitivity analysis in the next section.

5.2. Sensitivity analysis

Polynomial Chaos Expansion (PCE) is a powerful technique serving for analysis of uncertain systems, with applications in the domains of uncertainty quantification, reliability analysis, sensitivity analysis etc. This tools is exploited in this section in order to quantify the influence of variables on the prestressing effect. A PCE approximates the output of a system (computed prestress levels in the current study) as a polynomial expansion in terms of the defining input variables, as per Eq. (27). By projecting the system output onto a group of orthogonal polynomial bases, the PCE provides a set of coefficients that describe the system response. The UQLab [47] software, set up in a MATLAB environment is employed to construct the PCE for the sensitivity analysis. Interested readers are referred to relevant literature [47–49] for further details on the implementation and underpinning theory.

$$Y(\boldsymbol{X}) = \Sigma_{\alpha \in \mathcal{N}^d} y_\alpha \Psi_\alpha(\boldsymbol{X}) \qquad (27)$$

where $\boldsymbol{X}$ denotes a vector input variables; $Y(\boldsymbol{X})$ refers to the model output; y_α refers to the set of coefficients of the polynomial expansion $\Psi_\alpha(\boldsymbol{X})$.

Table 5
Random variable ranges and sensitivity indexes (total Sobol indexes).

Variables	L_{anchor} (mm)	L_{act} (mm)	σ_{rec} (MPa)	b_{SMA} (mm)
Ranges	[25, 300]	[25, 200]	[50, 400]	[25, 150]
Total Sobol indexes	0.000331	0.036971	0.572160	0.481475

When designing a bonded Fe-SMA strengthening system, the values of the four input variables are typically selected on the basis of engineering judgement. Therefore, uniform distributions are often assumed, and Legendre polynomials ($\Psi_\alpha(X)$) are utilized. Here, we adopt a PCE with a dimension of four (number of input variables) with a maximum polynomial degree of three, where the number of polynomial terms is $35 = \frac{(4+3)!}{4! \cdot 3!}$. The ordinary least square method, which requires data points $2 - 3$ times as the polynomial terms, is employed to compute the polynomial coefficients (y_α). Therefore, 120 steel plates strengthened by bonded Fe-SMA strips are analyzed, with values of four variables randomly generated within the ranges listed in Table 5. The prestress level of each strengthened plate is computed via the symmetric strengthening model, in terms of the compressive strain of the substrate plate. The coefficients (y_α) are obtained via substituting the model output ($Y(X)$, 120 strain values) and model input (X, 120 sets of four variables) into Eq. (27), along with an ordinary least square regression. 100 further strengthened plates are randomly generated to evaluate the established PCE model. A low leave-one-out error and validation error, which are 2.7×10^{-2} and 1.2×10^{-2}, respectively, confirm the quality of the established PCE model. The Sobol indexes, which describe the importance of variables to the model output, can be computed via Eq. (28). A larger Sobol index reflects a stronger influence of the variable on the model output.

$$S_{T,i} = \sum_{j,k=0}^{4} y_{ijk}^2 / \sum_{i,j,k=0}^{4} y_{ijk}^2 \tag{28}$$

where $S_{T,i}$ represents the total Sobol index of the ith variable; the term $\sum_{j,k=0}^{4} y_{ijk}^2$ corresponds to the sum of squares of coefficients associated with the ith variable, while $\sum_{i,j,k=0}^{4} y_{ijk}^2$ represents the sum of squares of all coefficients. Three footnotes i, j, and k indicate the maximum polynomial degree of three.

Table 5 lists the computed total Sobol index for each variable, which quantitatively characterizes the significance of the influence of each variable on the prestressing effect. Along with the parametric study in Section 5.1, the following can be summarized. (i) The recovery stress (σ_{rec}) and Fe-SMA strip width (b_{SMA}), which share similar importance, stand in the first position. They determine the maximum prestressing effect. (ii) The activation length (L_{act}), whose influence is capped by the recovery stress level (σ_{rec}), stands in the second position. It affects the final prestress level via the amount of prestress loss. (iii) The bonded anchorage length (L_{anchor}) is the least influential to the prestress level, however, a minimum length to resist the generated prestressing force should be guaranteed. It is worth noting that the "importance" here indicates how sensitive the final prestress level is to a variation in each variable (a gradient $\partial Y / \partial X_i$). Although the bonded anchorage length may seem less significant in varying the prestress level, it is in fact the foundation of the externally bonded Fe-SMA strengthening system. This makes the bonded anchorage zone a crucial and indispensable component.

6. Design recommendation and outlook

In this section, a design strategy is proposed for the strengthening of steel, glass, and RC structural members utilizing externally boned/near surface mounted Fe-SMA strips/rebars, based on the validated symmetric and asymmetric strengthening models.
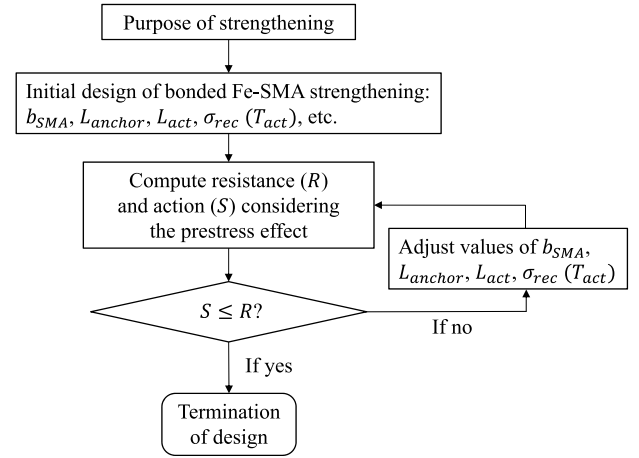

Fig. 11. Design flowchart, with examples of S and R listed in Table 6. Appendix C presents a practical design example of deflection control in a steel beam.

Table 6
Examples of design for strengthening.

Purposes of strengthening	Target features	Remark
Fatigue crack arrest[a]	$\Delta K_S \leq \Delta K_R$	ΔK: stress intensity range
Deformation control[b]	$\delta_S \leq \delta_R$	δ: Deformation of structure
Increase load capacity	$F_S \leq F_R$	F_S: External load, F_R: Capacity
Enhance cracking load[c]	$F_S \leq F_{cr,R}$	F_S: External load, $F_{cr,R}$: Cracking load

[a] Li et al. [11] provided an example of the fatigue crack arrest, where cracked steel plates were strengthened by bonded Fe-SMA strips, and the prestress analysis was conducted via the proposed symmetric strengthening model.

[b] Appendix C presents a practical design example that demonstrates the effective control of deflection in a steel beam. This is achieved by utilizing a bonded prestressed Fe-SMA strip.

[c] Rocha et al. [15] provided an analytical model for the computation of the cracking load of glass beams strengthened by bonded Fe-SMA strips.

6.1. General design concept

Generally, the purpose of the design is to guarantee that the resistance (R, also known as capacity) is no smaller than the action (S, also known as demand), as expressed in Eq. (29). To satisfy Eq. (29), a design strategy is outlined below and visualized in Fig. 11.

$$S \leq R \tag{29}$$

where S refers to as the action, while R represents the resistance.

1. Define the purpose of strengthening. Several examples are listed in Table 6.
2. Determine values of influential features, based on the engineering judgement.
3. Compute the action (S) and resistance (R) of a strengthened structure/member, considering the effect of applied prestress.
4. If the action (S) exceeds the resistance (R), adjust the influential features and return to step 3. The design of strengthening could be terminated when the action (S) no longer exceeds the resistance (R), i.e., Eq. (29) is satisfied.

When adjusting those influential features to improve the design, the steps illustrated in Fig. 12 are recommended, based on their importance. (i) A minimum bonded anchorage length (L_{anchor}) should be guaranteed, to hold the generated prestressing force and maintain a low prestress loss due to the deformation of adhesive joint. A longer bonded anchorage zone, though does not further enhance the prestressing effect, offers a greater bond capacity and improved joint ductility, which can serve as safety margins. An effective bond length (L_{eff})
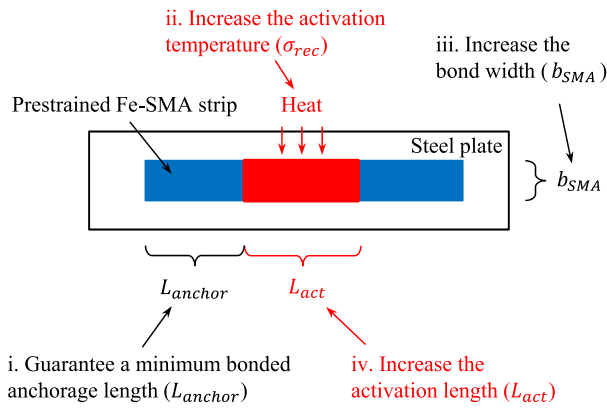
Fig. 12. Influential features to adjust (text in red color indicates an activation-temperature dependency). (For interpretation of the references to colour in this figure legend, the reader is referred to the web version of this article.)

could be employed, if the space allows. To enhance the prestressing effect, several approaches can be exploited: (ii) increasing the recovery stress level (σ_{rec}) by elevating the activation temperature (T_{act}), (iii) increasing the Fe-SMA strip width (b_{SMA}), and (iv) increasing the activation length (L_{act}). It is noteworthy that certain caps exist, as discussed previously.

Li et al. [11] realized arresting the fatigue crack growth of steel plates with central through-thickness cracks utilizing the bonded Fe-SMA strengthening. It is a good example of employing the recommended design model and strategy via tuning the recovery stress level (activation temperature). A further example of controlling the deflection of a steel beam is provided in Appendix C. The Fe-SMA strip width, activation length, and activation temperature are considered to improve the strengthening effect. In the meantime, geometrical boundary conditions, such as the beam span and beam width, are taken into consideration.

6.2. Recommendations for future studies

So far, all bonding and prestressing behaviors, which are used to construct the prestress analysis models, refer to short-term behaviors relying on a mild laboratory environment. In such an environment, (i) the applied load can be accurately measured, (ii) the activation temperature can be properly controlled, and (iii) adverse and long-term effects, which may degrade the bond behavior, are prevented in tests and ignored in the prestress analysis models. However, many adverse effects exist. The corrosion of Fe-SMA-adhesive interface in an harsh environment would degrade the bond capacity of the bonded anchorage zone [50], leading to premature failure of the strengthening system. During cycling loading, prestressed Fe-SMA strips experience a phase-transformation induced prestress loss [51], which worsens the prestressing effect. Other factors, which influence the long-term durability of CFRP bonded joints, might affect the Fe-SMA bond as well. These factors include freeze-thaw cycles [52–54], wetting-drying cycles [55,56], and elevated temperature during summer [33,57–59].

Apart from the above-mentioned adverse effects, intrinsic uncertainties exist in both the action and resistance. Therefore, the deterministic model, as written per Eq. (29), could be replaced by a semi-probabilistic model, Eq. (30), which is in line with Eurocode 0 [60].

$$S_{rep} \cdot \gamma_{Sd} \leq \frac{R\{\eta \cdot \frac{X_k}{\gamma_m}\}}{\gamma_{Rd}} \tag{30}$$

where S_{rep} is the representative value of the action; γ_{Sd} is the partial factor taking account of the uncertainties in the actions; $R\{\cdot\}$ is the resistance; X_k is the characteristic value of the material property; γ_m represents the material partial factor, taking account of material

uncertainties, such as the recovery stress level; the conversion factor η considers the aforementioned adverse effects, such as the corrosion to the bonding interface; γ_{Rd} is a partial factor covering the uncertainty of the resistance model.

The left side of Eq. (30) could be the external load, while the right side is the load capacity of a structure after strengthening. Another example could be that the left side is the deflection considering material uncertainties etc., with some terms shifted to the left side, while the right side reflects a predefined allowable constant value. Note, that "action" and "effect of action" are not distinguished here, for the sake of simplicity. The uncertainty in the geometry, which could play a role in some cases, is not involved in the discussion. However, in engineering design, "action" and "effect of action" should be distinguished, while geometric uncertainties should be considered as well.

Since bonding Fe-SMA strips barely affects the geometries of existing structures and loading types, the partial factor on the action side (γ_{Sd}) can be referred to Eurocode [60] or local standards. Further investigations are required to quantify (i) conversion factors (η), representing the adverse effects, (ii) characteristic values of Fe-SMA (X_k), such as the recovery stress values at different activation temperatures, (iii) the partial factor for the Fe-SMA material (γ_m), and (iv) the partial factor for the bonded Fe-SMA strengthening system (γ_{Rd}). For inspiration purpose, interested readers are referred to an Italian guideline [61] for the design of externally bonded FRP strengthening system.

7. Conclusion

In this study, a symmetric, asymmetric, and modified asymmetric strengthening models are proposed for assessing the strengthening efficiency of structures strengthened by bonded Fe-SMA strips; these models are validated through the experimentally measured strains and deflections of strengthened steel, glass, and reinforced concrete (RC) structural members. Subsequently, a parametric study and a sensitivity analysis are conducted based on the validated symmetric strengthening model. Finally, a design recommendation is proposed, along with an outlook involving possible future investigations. The following can be summarized:

1. The proposed models can predict the prestress levels (in terms of compressive strains in substrates) and deflections of experimentally tested steel, glass, and RC structural members with a fairly good accuracy, proving the generality of the proposed models and methodology of analysis. This suggests a potential of employing the proposed models in design of steel, glass, and RC structures strengthened by externally bonded/near surface mounted Fe-SMA strips/rebars.
2. The four influential variables that significantly affect the prestressing effect are ranked in the following order: recovery stress (σ_{rec}) $\approx$ Fe-SMA width (b_{SMA}) > activation length (L_{act}) > bonded anchorage length (L_{anchor}). Ensuring a minimum bonded anchorage length is essential to retain the prestressing force, preventing the bonded strengthening system failure during activation.
3. To reach an optimized strengthening effect, when designing an externally boned Fe-SMA strengthening system, the four influential features can be tuned according to their importance (as in point 2) and the boundary conditions (such as geometric limitations).
4. A semi-probabilistic design model, which is in line with Eurocode 0, is further outlined. Further investigations are required to assess adverse effects, such as the degraded bond behavior in harsh environments, and for quantifying the uncertainties in the bonded/embedded Fe-SMA strengthening system.
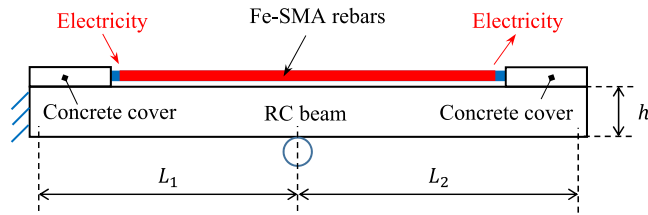
Fig. A.13. Schematic view of a RC beam strengthened by Fe-SMA rebars. The exposed Fe-SMA rebars are covered by mortar after the activation test.
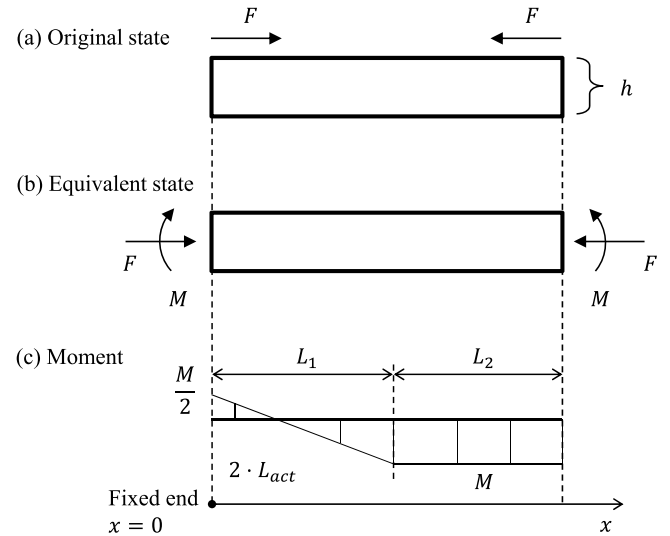

Fig. A.14. Analysis of force and deformation in the RC beam. In this simplified model, the activation length is assumed being identical to the entire beam length, despite the former being shorter than the latter. Fig. 10(b) suggests that varying a long activation length has a marginal effect to the prestress level.

Appendix A. Strengthening model for RC beams with specific boundary conditions

The symmetric and asymmetric strengthening models are applicable to RC structures. Nevertheless, RC structures strengthened by Fe-SMA, as documented in current literature [37] and illustrated in Fig. A.13, exhibit boundary conditions distinct from those stipulated in the symmetric and asymmetric strengthening models. Consequently, a supplementary asymmetric strengthening model is formulated in this Appendix. Since Schranz et al. [37] observed no visible cracks in the RC beams during the activation stage, plasticity and cracking of concrete are excluded in our model analysis. It is important to note that, unless otherwise specified, the meanings of variables in this Appendix remain identical to those in the asymmetric strengthening model.

Considering the applied prestressing force as an external load acting on the RC beam, as illustrated in Fig. A.14, the prestressing force and resulting moment read:

$$F = \sigma_{pre} \cdot A_{SMA} \tag{A.1}$$

$$M = F \cdot \frac{h}{2} \tag{A.2}$$

The tip deflection reads (a classical solution in text books of Structural Analysis):

$$w = -\frac{M \cdot L_1 \cdot L_2}{4 E_c \cdot I} \cdot (1 + 2 \cdot \frac{L_2}{L_1}) \tag{A.3}$$

where w refers to the tip deflection, with a negative sign reflecting an upward deflection; E_c and I denote the E-modulus and moment of inertia of the unstrengthened concrete beam, respectively.

The strain component resulting from the compression of the RC beam reads:

$$\varepsilon_{comp} = \frac{F}{A_c \cdot E_c} \tag{A.4}$$

where A_c refers to the cross-sectional area of the unstrengthened concrete beam.

The moment acting on an arbitrary cross-section reads:

$$M(x) = \begin{cases} -\frac{M}{2} + \frac{3 \cdot M}{2 \cdot L_1} \cdot x, \text{if } 0 \leq x \leq L_1 \\ M, \text{if } L_1 < x \leq L_1 + L_2 \end{cases} \tag{A.5}$$

The bending strain at the beam edge reads:

$$\varepsilon_{bending}(x) = \frac{M(x) \cdot h/2}{E_c \cdot I} \tag{A.6}$$

Substituting Eq. (A.5) into Eq. (A.6) yields:

$$\varepsilon_{bending}(x) = \begin{cases} -\frac{M \cdot h}{4 \cdot E_c \cdot I} + \frac{3 \cdot M \cdot h}{4 \cdot E_c \cdot I \cdot L_1} \cdot x, \text{if } 0 \leq x \leq L_1 \\ \frac{M \cdot h}{2 \cdot E_c \cdot I}, \text{if } L_1 < x \leq L_1 + L_2 \end{cases} \tag{A.7}$$

The three major contributors of prestress loss are (i) compression of the RC beam, (ii) deflection of the RC beam, and (iii) slip of the Fe-SMA-to-mortar joint. Therefore, the prestress loss marks:

$$\sigma_{loss} = [\varepsilon_{comp} + \frac{\int_0^{L_1+L_2} \varepsilon_{bending}(x)\mathrm{d}x}{L_1 + L_2} + \frac{2 \cdot \Delta_a}{L_1 + L_2}] \cdot E_{SMA} \tag{A.8}$$

where the slip of the Fe-SMA-to-mortar joint can be estimated as:

$$\Delta_a = \frac{\sigma_{pre} \cdot A^*_{SMA}}{k_{joint}} \tag{A.9}$$

where A^*_{SMA} refers to the cross-sectional area of a single Fe-SMA rebar; k_{joint} represents the loading stiffness of Fe-SMA-to-mortar joint, which is calculated via a model proposed by Li et al. [29].

The prestress is again estimated as the subtraction of recovery stress by the prestress loss:

$$\sigma_{pre} = \sigma_{rec} - \sigma_{loss} \tag{A.10}$$

Substituting Eqs. (A.1), (A.2), (A.4) and (A.7) to (A.9) into Eq. (A.10) yields the analytical solution of the prestress loss and final

Table B.7
Experimental measurements and modeling results.

	Specimen symbol	Exp. strain ($\mu\varepsilon$)	Exp. deflection (mm)	Model strain ($\mu\varepsilon$)	Model deflection (mm)	σ_{rec} (MPa)	σ_{pre} (MPa)	$1-\frac{\sigma_{pre}}{\sigma_{rec}}$
Steel plates [21]	S-100	−39.1	N/A	−52	N/A	230	106	54%
	SC-100	−67.5		−72		320	147	36%
	SC-200	−86.2		−102		320	209	35%
	S-300	−80.3		−112		320	231	28%
	SC-300	−103.4		−112		320	231	28%
	SC-500	−123.1		−125		320	257	20%
Steel plates [11]	SP-Act120	−161	N/A	−160	N/A	230	164	29%
	SP-Act180	−192		−222		320	229	28%
	SP-Act260–1	−171[a]		−277		400	285	29%
	SP-Act260–2	−157[a]		−277		400	285	29%
Glass plates [14]	BT-10-SP-a	−82.5[b]	N/A	−104.6	N/A	300	262	13%
	BT-11-SP-a	−95.6[b]		−104.6		300	262	13%
	BT-12-SP-a	−108.7[b]		−104.6		300	262	13%
Steel beams [12,13]	SB-part	20.2[c] −68.5[d]	1	19.7[c] −86.2[d]	1.20	324	309	5%
	SB-full	13[c] −49.3[d]	0.73	17.1[c] −75[d]	1.05	283	270	5%
Glass beams [15]	P_T120-I	69[c]	0.433	51[c]	0.332	201.7	139	31%
	P_T120-II	71[c]	0.445	52[c]	0.341	207	143	31%
	P_T140	91[c]	0.584	66[c]	0.435	263.8	182	31%
	P_T160	115[c]	0.752	89[c]	0.585	355.2	245	31%
RC beams [37]	2-CR-act	58[d]	3.3	43[d]	2.6	340	322	5%
	4-NSM-act	N/A	2.0	N/A	2.4	330	313	5%

[a] Strain measurements are regarded as inaccurate due to the temperature of the substrate steel plates exceeding the temperature range of strain gauges.

[b] Only the mean value (μ_ε) and standard deviation (σ_ε) of three measurements are available in the literature. Values of $\mu_\varepsilon - \sigma_\varepsilon \cdot \sqrt{3/2}$, μ_ε, and $\mu_\varepsilon + \sigma_\varepsilon \cdot \sqrt{3/2}$ are adopted as the experimental measurements.

[c] Strain at upper flange or edge.

[d] Strain at lower flange or edge.

Table C.8
An example of bonded Fe-SMA strengthening.

Iteration number	L_{act} (mm)	L_{SMA} (mm)	L_{grad} (mm)	b_{SMA} (mm)	T_{act} (°C)	σ_{rec} (MPa)	δ_S (mm)	Action	$\delta_S \in [4, 16]$?	τ_{max}[a] (MPa)
1	500	1480	2000	25	120	230	1.69	Initial design	No	12
2	500	1480	2000	50	120	230	3.37	Increasing b_{SMA}	No	12
3	1000	2480	1500	50	120	230	3.85	Increasing L_{act}	No	12
4	1000	2480	1500	50	180	320	5.35	Increasing T_{act}	Yes	19
5	1500	3480	1000	50	180	320	5.80	Increasing L_{act}	Yes	19
6	1500	3480	1000	50	260	400	7.25	Increasing T_{act}	Yes	20
7	2000	4480	500	50	260	400	7.58	Increasing L_{act}	Yes	20

* Since the space allows, a $L_{anchor} = 240$ mm, which is approximately twice the effective bond length, is assigned for all design cases.

** The Fe-SMA strip length ($L_{SMA} = 2 \cdot L_{act} + 2 \cdot L_{anchor}$) should not exceed the beam span, which is 5000 mm.

[a] τ_{max} refers to the maximum shear stress in the bond line resulting from activation, determined via a numerical model from Ref. [29]. $\tau_{max} \geq 20$ MPa suggests a damage accumulation in the bond line.

prestress level:

$$\sigma_{pre} = \frac{\sigma_{rec}}{1 + \underbrace{\frac{A_{SMA} \cdot E_{SMA}}{A_c \cdot E_c}}_{\text{compression term}} + \underbrace{\frac{A_{SMA} \cdot E_{SMA} \cdot h^2}{E_c \cdot I} \cdot \frac{4 \cdot L_2 - 3 \cdot L_1}{16 \cdot (L_1 + L_2)}}_{\text{bending term}} + \underbrace{\frac{2 \cdot A^*_{SMA} \cdot E_{SMA}}{k_{joint} \cdot (L_1 + L_2)}}_{\text{joint slip term}}}$$

(A.11)

Appendix B. Experimental measurements and modeling results

A comprehensive comparison of strains and deflections obtained from experimental measurements and modeling results is provided in Table B.7.

Appendix C. An example of bonded Fe-SMA strengthening for a steel beam

This section provides an example of designing a bonded Fe-SMA strengthening for a steel beam, which is schematically illustrated in Fig. C.15. The downward deflection of this steel beam with a crane
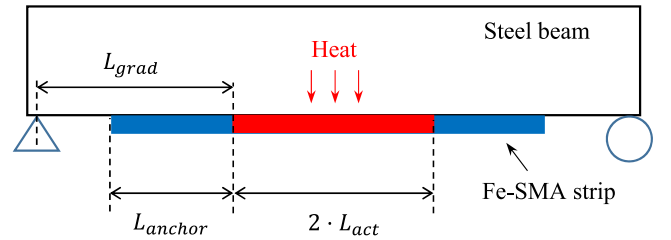

Fig. C.15. A steel beam with a span of 5 m strengthened by a bonded prestressed Fe-SMA strip. $h = 120$ mm, flange width = 58 mm, $E_{steel} = 200$ GPa, $A_{steel} = 1420$ mm², $I = 3,280,000$ mm⁴. Variables are: T_{act}, L_{act}, L_{anchor}, and b_{SMA}.

rail has exceeded a limitation. Therefore, the steel beam is required to deform at least 4 mm upward, to ensure a smooth daily operation. In the meantime, the upward deflection should be less than 16 mm.

The steel beam of type INP120 has a span of 5 m, a beam height of $h = 120$ mm, a flange width of 58 mm, an E-modulus of $E_{steel} = 200$ GPa,

a cross-sectional area of $A_{steel} = 1420$ mm^2, and a moment of inertial of $I = 3,280,000$ mm^4. An iterative design procedure is presented in Table C.8. Focusing exclusively on the upward deflection criterion of $\delta_S \in [4, 16]$, strengthening designs at iterations 1−3 are insufficient to control the beam deflection, while iterations 4−7 are appropriate. A maximum $b_{SMA} = 50$ mm is employed in the design, as a single Fe-SMA strip width (b_{SMA}) should not exceed the beam width of 58 mm. Engineers may consider to bond further narrower Fe-SMA strips on the upper surface of the lower flange to reach a stronger strengthening effect. Notably, adhesive damage arises during iterations 6−7, reflected by $\tau_{max} = 20$ MPa. Careful consideration is required when increasing the recovery stress (σ_{rec}) by elevating the activation temperature, as it may result in a heat-induced bonding property degradation [30,62].

References

[1] Ghafoori E. Editorial for special issue on sustainable metallic structures. Eng Struct 2019;183:83.

[2] Hertwich EG, Ali S, Ciacci L, Fishman T, Heeren N, Masanet E, Asghari FN, Olivetti E, Pauliuk S, Tu Q, et al. Material efficiency strategies to reducing greenhouse gas emissions associated with buildings, vehicles, and electronics—a review. Environ Res Lett 2019;14(4):043004.

[3] Hong T, Ji C, Jang M, Park H. Assessment model for energy consumption and greenhouse gas emissions during building construction. J Manage Eng 2014;30(2):226–35.

[4] Hosseini E, Ghafoori E, Leinenbach C, Motavalli M, Holdsworth SR. Stress recovery and cyclic behaviour of an Fe–Mn–Si shape memory alloy after multiple thermal activation. Smart Mater Struct 2018;27(2):025009.

[5] Hosseini A, Michels J, Izadi M, Ghafoori E. A comparative study between Fe-SMA and CFRP reinforcements for prestressed strengthening of metallic structures. Constr Build Mater 2019;226:976–92.

[6] Izadi M, Ghafoori E, Motavalli M, Maalek S. Iron-based shape memory alloy for the fatigue strengthening of cracked steel plates: Effects of re-activations and loading frequencies. Eng Struct 2018;176:953–67.

[7] Gu X-L, Chen Z-Y, Yu Q-Q, Ghafoori E. Stress recovery behavior of an Fe-Mn-Si shape memory alloy. Eng Struct 2021;243:112710.

[8] Chen Z-Y, Gu X-L, Zhao X-L, Ghafoori E, Yu Q-Q. Fatigue tests on Fe-SMA strengthened steel plates considering thermal effects. J Struct Eng 2023;149(3):04022255.

[9] Fritsch E, Izadi M, Ghafoori E. Development of nail-anchor strengthening system with iron-based shape memory alloy (Fe-SMA) strips. Constr Build Mater 2019;229:117042.

[10] Wang W, Li L, Hosseini A, Ghafoori E. Novel fatigue strengthening solution for metallic structures using adhesively bonded Fe-SMA strips: A proof of concept study. Int J Fatigue 2021;148:106237.

[11] Li L, Wang S, Chen T, Chatzi E, Heydarinouri H, Ghafoori E. Fatigue strengthening of cracked steel plates with bonded Fe-SMA strips, vol. 6, Wiley Online Library; 2023, p. 380–4.

[12] Wang S, Li L, Su Q, Jiang X, Ghafoori E. Strengthening of steel beams with adhesively bonded memory-steel strips. Thin-Walled Struct 2023;189:110901.

[13] Wang S, Li L, Su Q, Jiang X, Ghafoori E. Experimental study on steel girder strengthened with adhesively bonded iron-based shape memory alloy. In: The sixth international conference on smart monitoring, assessment and rehabilitation of civil structures. SMAR 2022, Shanghai, China; 2022.

[14] Silvestru V-A, Deng Z, Michels J, Taras A. Enabling a ductile failure of laminated glass beams with iron-based shape memory alloy (Fe-SMA) strips. Ce/papers 2022;5(4):948–56.

[15] Rocha J, Pereira E, Sena-Cruz J. Feasibility of mechanical post-tensioning of annealed glass beams by activating externally bonded Fe-SMA reinforcement. Constr Build Mater 2023;365:129953.

[16] Dong Z, Klotz UE, Leinenbach C, Bergamini A, Czaderski C, Motavalli M. A novel Fe-Mn-Si shape memory alloy with improved shape recovery properties by VC precipitation. Adv Eng Mater 2009;11(1–2):40–4.

[17] Koster M, Lee W, Schwarzenberger M, Leinenbach C. Cyclic deformation and structural fatigue behavior of an FE–Mn–Si shape memory alloy. Mater Sci Eng A 2015;637:29–39.

[18] Cladera A, Weber B, Leinenbach C, Czaderski C, Shahverdi M, Motavalli M. Iron-based shape memory alloys for civil engineering structures: An overview. Constr Build Mater 2014;63:281–93.

[19] Fang C, Wang W, Ji Y, Yam MC. Superior low-cycle fatigue performance of iron-based SMA for seismic damping application. J Constr Steel Res 2021;184:106817.

[20] Sawaguchi T, Sahu P, Kikuchi T, Ogawa K, Kajiwara S, Kushibe A, Higashino M, Ogawa T. Vibration mitigation by the reversible fcc/hcp martensitic transformation during cyclic tension–compression loading of an Fe–Mn–Si-based shape memory alloy. Scr Mater 2006;54(11):1885–90.

[21] Wang S, Su Q, Jiang X, Li L, Motavalli M, Ghafoori E. Compact self-prestressing Fe-SMA/CFRP bonded patches for repair of fatigue cracks. 2023, In preparation, invited by Construction and Building Materials.

[22] Michels J, Sena-Cruz J, Czaderski C, Motavalli M. Structural strengthening with prestressed CFRP strips with gradient anchorage. J Compos Constr 2013;17(5):651–61.

[23] Yang J, Haghani R, Al-Emrani M. Innovative prestressing method for externally bonded CFRP laminates without mechanical anchorage. Eng Struct 2019;197:109416.

[24] Rezazadeh M, Barros J, Costa I. Analytical approach for the flexural analysis of RC beams strengthened with prestressed CFRP. Composites B 2015;73:16–34.

[25] Shahverdi M, Czaderski C, Motavalli M. Iron-based shape memory alloys for prestressed near-surface mounted strengthening of reinforced concrete beams. Constr Build Mater 2016;112:28–38.

[26] Hong K-N, Yeon Y-M, Ji S-W, Lee S. Flexural behavior of RC beams using Fe-based shape memory alloy rebars as tensile reinforcement. Buildings 2022;12(2):190.

[27] Rojob H, El-Hacha R. Self-prestressing using iron-based shape memory alloy for flexural strengthening of reinforced concrete beams. ACI Struct J 2017;114(2):523.

[28] Li L, Wang W, Chatzi E, Ghafoori E. Experimental investigation on debonding behavior of Fe-SMA-to-steel joints. Constr Build Mater 2023;364:129857.

[29] Li L, Chatzi E, Ghafoori E. Debonding model for nonlinear Fe-SMA strips bonded with nonlinear adhesives. Eng Fract Mech 2023;109201.

[30] Li L, Chatzi E, Czaderski C, Ghafoori E. Influence of activation temperature and prestress on behavior of Fe-SMA bonded joints. Constr Build Mater 2023;409:134070.

[31] Sika AG. Additional product information, SikaPower-1277, version 1. 2018.

[32] Sika AG. Additional product information, SikaPower-1277, version 2. 2018.

[33] He J, Xian G, Zhang Y. Effect of moderately elevated temperatures on bond behaviour of CFRP-to-steel bonded joints using different adhesives. Constr Build Mater 2020;241:118057.

[34] Qiang X, Wu Y, Wang Y, Jiang X. Novel crack repair method of steel bridge diaphragm employing Fe-SMA. Eng Struct 2023;292:116548.

[35] Mohri M, Leinenbach C, Lignos DG, Ghafoori E. Effect of heat treatment on microstructure and pseudoelasticity of a memory-steel. Ce/papers 2023;6(3–4):633–8.

[36] Izadi M, Ghafoori E, Shahverdi M, Motavalli M, Maalek S. Development of an iron-based shape memory alloy (Fe-SMA) strengthening system for steel plates. Eng Struct 2018;174:433–46.

[37] Schranz B, Michels J, Czaderski C, Motavalli M, Vogel T, Shahverdi M. Strengthening and prestressing of bridge decks with ribbed iron-based shape memory alloy bars. Eng Struct 2021;241:112467.

[38] Fernando ND, et al. Bond behaviour and debonding failures in CFRP-strengthened steel members. 2010.

[39] Wang H-T, Wu G. Bond-slip models for CFRP plates externally bonded to steel substrates. Compos Struct 2018;184:1204–14.

[40] Jiang C, Yu Q-Q, Gu X-L. A unified bond-slip model for the interface between FRP and steel. Composites B 2021;227:109380.

[41] Shahverdi M, Michels J, Czaderski C, Motavalli M. Iron-based shape memory alloy strips for strengthening RC members: Material behavior and characterization. Constr Build Mater 2018;173:586–99.

[42] Callewaert D, Belis J, Delincé D, Van Impe R. Experimental stiffness characterisation of glass/ionomer laminates for structural applications. Constr Build Mater 2012;37:685–92.

[43] Pankhardt K. Temperature dependent flexural stiffness of load bearing laminated glass panes. Period Polytech Civ Eng 2010;54(2):117–26.

[44] Biolzi L, Ghittoni C, Fedele R, Rosati G. Experimental and theoretical issues in FRP-concrete bonding. Constr Build Mater 2013;41:182–90.

[45] Dai J, Ueda T, Sato Y. Development of the nonlinear bond stress–slip model of fiber reinforced plastics sheet–concrete interfaces with a simple method. J Compos Constr 2005;9(1):52–62.

[46] Wu Z, Yuan H, Niu H. Stress transfer and fracture propagation in different kinds of adhesive joints. J Eng Mech 2002;128(5):562–73.

[47] Marelli S, Sudret B. UQLab user manual – Polynomial chaos expansions. Tech. rep, Switzerland: Chair of Risk, Safety and Uncertainty Quantification, ETH Zurich; 2021, Report # UQLab-V1.4-104.

[48] Torre E, Marelli S, Embrechts P, Sudret B. Data-driven polynomial chaos expansion for machine learning regression. J Comput Phys 2019;388:601–23.

[49] Sudret B. Global sensitivity analysis using polynomial chaos expansions. Reliab Eng Syst Saf 2008;93(7):964–79.

[50] Pichler N, Wang W, Poulis JA, Ghafoori E. Surface preparations and durability of iron-based shape memory alloy adhesively-bonded joints. Int J Adhes Adhes 2023;125:103439.

[51] Ghafoori E, Hosseini E, Leinenbach C, Michels J, Motavalli M. Fatigue behavior of a Fe-Mn-Si shape memory alloy used for prestressed strengthening. Mater Des 2017;133:349–62.

[52] Agarwal A, Foster SJ, Hamed E, Ng TS. Influence of freeze–thaw cycling on the bond strength of steel–FRP lap joints. Composites B 2014;60:178–85.

[53] Pang Y, Wu G, Wang H, Liu Y. Interfacial bond-slip degradation relationship between CFRP plate and steel plate under freeze-thaw cycles. Constr Build Mater 2019;214:242–53.

[54] Heshmati M, Haghani R, Al-Emrani M. Durability of bonded FRP-to-steel joints: Effects of moisture, de-icing salt solution, temperature and FRP type. Composites B 2017;119:153–67.

[55] Heshmati M, Haghani R, Al-Emrani M. Durability of CFRP/steel joints under cyclic wet-dry and freeze-thaw conditions. Composites B 2017;126:211–26.

[56] Dawood M, Rizkalla S. Environmental durability of a CFRP system for strengthening steel structures. Constr Build Mater 2010;24(9):1682–9.

[57] Zhou H, Fernando D, Torero JL, Torres JP, Maluk C, Emberley R. Bond behavior of CFRP-to-steel bonded joints at mild temperatures: experimental study. J Compos Constr 2020;24(6):04020070.

[58] Feng P, Hu L, Zhao X-L, Cheng L, Xu S. Study on thermal effects on fatigue behavior of cracked steel plates strengthened by CFRP sheets. Thin-Walled Struct 2014;82:311–20.

[59] Breveglieri M, Czaderski C. Reinforced concrete slabs strengthened with externally bonded carbon fibre-reinforced polymer strips under long-term environmental exposure and sustained loading. Part 1: Outdoor experiments. Composites C 2022;7:100239.

[60] Standard B. Eurocode 0: Basis of structural design. Eurocode 2002.

[61] CNR. Guidelines for the design and construction of externally bonded FRP systems for strengthening existing structures. Metallic structures. Preliminary study. 2005.

[62] Liu Z, Dong Z, Sun Y, Zhu H, Wu G, Sun C, Soh C-K. Effect of resistive heating on the bond properties between iron-based shape memory bars and cement mortar. J Build Eng 2023;66:105895.